

LASER SENSING OF THE LAKE BAIKAL WATERS

G.P. Kokhanenko,¹ I.E. Penner,¹ V.S. Shamanaev,¹ G. Ladbrook,² and A. Scott²

¹*Institute of Atmospheric Optics,
Siberian Branch of the Russian Academy of Sciences, Tomsk*

²*DERA, Malvern, Great Britain*

Received October 27, 1998

The results of airborne sensing of the Lake Baikal waters and the atmosphere over it are discussed. The results have been obtained in November of 1996 during the flight of AN-30 OPTIK-E aircraft-laboratory with onboard lidar over Lake Baikal. The results presented demonstrate some specific features of lidar returns and the possibilities of data processing. For pure water in the northern part of Lake Baikal, the measured extinction coefficient is $0.12 \pm 0.01 \text{ m}^{-1}$, while near the Selenga mouth it varies from 0.14 to 0.6 m^{-1} . The minimum and maximum depths measurable with the lidar are estimated. The depth of 40 m was fixed near B. Ushkanii Island.

1. INTRODUCTION

Lidars are widely used for water turbidity and depth sensing. The MAKREL-2 lidar developed at the Institute of Atmospheric Optics of SB RAS has been in use since 80s for water monitoring and detecting fish shoals in Norway, Barents, North, and other seas.

Lake Baikal is also a good object for lidar measurements. It is the largest reservoir of fresh water in the world. Its area ($600 \times 80 \text{ km}^2$) allows the Lake Baikal to be classified as a small-size internal sea. Various airborne studies of the Baikal environment and waters have already been conducted earlier.^{1,2} Measurements of water turbidity are of interest for ecological purposes. Besides, they allow final development of the technique of lidar sensing because of a very wide variability range of water transparency in the upper water layer starting from very turbid water of Selenga River, flowing into Lake Baikal, up to very pure water with the extinction coefficient only slightly increasing that for Sargasso Sea known as having the most transparent water in the world.

The AN-30 OPTIK-E aircraft-laboratory of the Institute of Atmospheric Optics, SB RAS,³ with the versatile airborne MAKREL-2 lidar was flying over Lake Baikal in November of 1996. The flight height was typically about 300 m. The lidar was equipped with a 150-mm-diameter telescope and a Nd:YAG laser operating at the wavelength of $0.53 \mu\text{m}$ and having the pulse power of 50 mJ. The laser radiation was linearly polarized. Two receiving channels (for the polarized and cross-polarized components) and two photoelectric multipliers FEU-144 were used as photodetectors. The electronics of 32 MHz pass band (taking into account the characteristics of a 7-bit ADC used) was used in the recording system, the discretization interval of 7.5 ns corresponds to the

vertical underwater resolution of 0.84 m. The pulse repetition rate up to 25 Hz provided the horizontal resolution of 4 m. The independent automated Global Positioning System (GPS) served to determine the aircraft position. Figure 1 shows a part of our route above the Selenga delta.

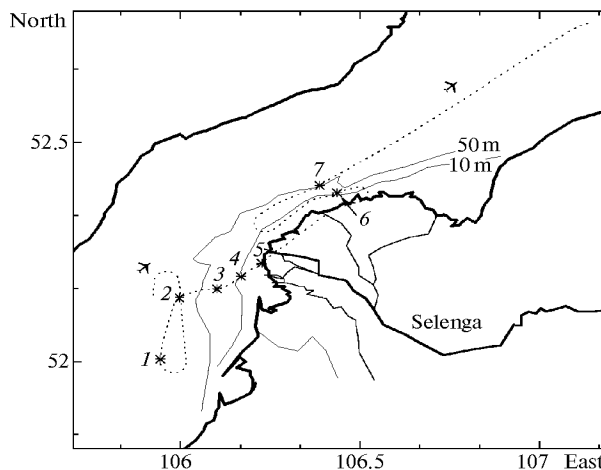


FIG. 1. A part of the flight route above the Selenga delta. The numbered stars correspond to the route points shown in Fig. 3.

2. ALGORITHMS FOR LIDAR RETURN PROCESSING

The algorithms used for extracting the information about optical properties of water are usually based on the single scattering approximation. The equation of lidar sensing (ELS) that relates the

power characteristics of a lidar return signal to the optical parameters of a water medium is as follows:

$$P(r) = \frac{C}{(H_0 + r/n)^2} \sigma_\pi(r) \exp\left(-2 \int_0^r \varepsilon(r') dr'\right). \quad (1)$$

Here σ_π is the backscattering coefficient; ε is the extinction coefficient; H_0 is the distance from the lidar to the water surface; r is the water depth. For an airborne lidar, H_0 is typically several hundred meters. In this case, the lidar overlap function is already formed in the atmospheric part of the path and under the water the return signal obeys the law of inverse squares (r^{-2}).

The simplest approximation when solving ELS for the case of homogeneous scattering medium is the logarithmic derivative method. Its main condition to be fulfilled is that $\sigma_\pi(r)$ and $\varepsilon(r)$ are constants. In this case, the depth average extinction coefficient ε is estimated from the back slope of the signal on the logarithmic scale. For signal digitizing a 7-bit ADC was used. Upon digitizing the data from every channel form an array of 128 points P_i with the values from 0 to 127. The digitization error is ± 1 least significant digit.

Let $i_1 \dots i_n$ be the sequence of digitizing points, and $P_1 \dots P_n$ be the corresponding digitized values of a signal. If S_i are the values of the lidar function $S(r) = P(r)(H_0 + r/n)^2$ at the corresponding points r_i , then the path mean extinction coefficient ε can be estimated using the method of least squares:

$$\varepsilon = 0.5 \frac{\sum_{i_1}^{i_2} r_i \sum_{i_1}^{i_2} \ln S_i - (i_2 - i_1 + 1) \sum_{i_1}^{i_2} r_i \ln S_i}{\left(\sum_{i_1}^{i_2} r_i\right)^2 - (i_2 - i_1 + 1) \sum_{i_1}^{i_2} r_i^2}. \quad (2)$$

For every pulse we selected the initial point i_1 at the 90-% level of the ADC dynamic range ($P(i_1) \leq 110$ units). At the end of the processed interval (point i_2) the signal value must, at least, exceed the ADC noise level. We used the value $P(i_2) = 3$ units, i.e. the signal-to-noise ratio was above three. As a rule, the interval $i_1 - i_2$ corresponded to depths of 5–15 m but varied in different measurement sessions, because it depended on water turbidity and signal power. Besides, signals were controlled to prevent inclusion of PMT afterpulses into the processing.

It is assumed in ELS (1) that the medium is irradiated by an infinitely short δ -pulse and the recording system immediately responds to the incident pulses. Real laser pulse has a finite length comparable to time resolution of the receiving system and with the extinction length in a scattering medium. So some correction is needed for ELS in its simplest form. As known, for a linear receiving system⁵ the resulting signal $U(t)$ is determined as a convolution of the lidar

signal $P(t)$ given by Eq. (1) and the pulse transient function (PTF) of the system $H(t)$:

$$U(t) = H(t) * P(t) = \int_0^t H(t - \tau) P(\tau) d\tau. \quad (3)$$

The system's PTF is governed by several factors: finite time resolution of a PMT, shape of a laser pulse, ADC pass band, and others. For purposes of lidar sensing, the PTF can be measured experimentally in a rather simple way: from a signal backscattered by a plane surface (we used the wall of the building 50 m far). Because in this case $P(t) \equiv \delta(t)$, the recorded signal $U(t)$ was equal to $H(t)$. Then Eq. (3) can be solved using one of known methods for signal reconstruction which are especially well developed for the convolution equation.^{6,7} (The halfwidth of the measured $H(t)$ is about 16 ns, and its fall off is similar to the exponential decay of the lidar signal at the medium extinction coefficient $\varepsilon = 0.6 \text{ m}^{-1}$. It is clear that, when sensing such a dense medium as water, where the values of ε may be on the same order of magnitude or even exceeding this value, the time resolution of the system should necessarily be taken into account).

The medium is assumed to be *a priori* homogeneous in the logarithmic derivative method (2), i.e., a particular model of $\varepsilon(r)$ distribution is already set. So the iteration procedure is most convenient way to solve Eq. (3) in which the time lag is taken into account. The value ε^0 found from substitution of the measured signal $U(t)$ for $p^0(t)$ in Eq. (2) is taken as the initial approximation. At every next iteration step, it is taken that $\varepsilon_i = k\varepsilon_{i-1}$. The value $k = 1.05$ results from a 5-% error of ε calculation by Eq. (2). The lidar signal $P_i(t)$ is calculated by Eq. (1), and the recorded signal $U_i(t) = H(t) * P_i(t)$. The iteration process continues until the deviation $\|U_i(t) - U_{i-1}(t)\|$ becomes less than 10%.

The calculations have shown that for slowly decreasing signals (when $\varepsilon < 0.3 \text{ m}^{-1}$ in water) the iteration procedure terminates already at the first step. This means that the calculated parameter ε_0 does not require further corrections. Figure 2 presents the results obtained by applying this procedure to analysis of turbid water. The data were obtained during the flight over the point 6 (see Fig. 1), where the depth decreases sharply from 50 to 10 m. The closed squares here demonstrate the values of ε_0 without any correction, while the circles are for the results calculated through application of the iteration procedure. It is seen that at $\varepsilon_0 < 0.35 \text{ m}^{-1}$ there is no need for any temporal correction. Near the center (see Fig. 2) $\varepsilon_0 = 0.51 \pm 0.04$ without a correction and the corrected value $\varepsilon = 0.66 \pm 0.07$. Although the relative discrepancy between the data has increased, the error in ε markedly exceeds the measurement error. It should be noted that in a more turbid water the error of ε calculation by Eq. (2) increases rapidly because of a decrease in the number of digitized points in the

$i_1 - i_2$ interval. Errors necessarily arise in the experimental measurements of PTF $H(t)$ as well. These circumstances restrict the upper limit of water turbidity (i.e., the maximum value of ϵ) which can be measured with a lidar. For example, formal processing of signals recorded when flying over the shore line gives $\epsilon_0 = 0.8 \pm 0.2$ (averaged over 100 pulses).

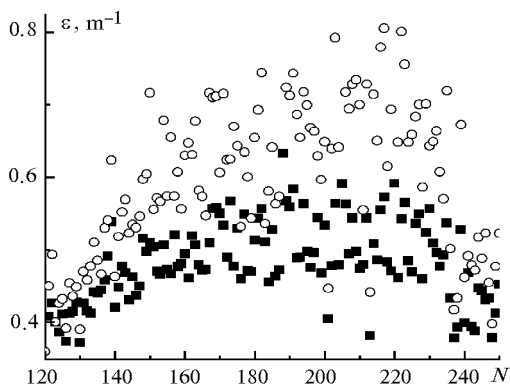


FIG. 2. The values of the extinction coefficient reconstructed from signals recorded during the flight over polluted water; N is the running number of a laser pulse: processing of not corrected, "raw" return signals (squares), processing with regard for the lidar pulse transient function (circles).

Thus, the value $\epsilon_0 = 0.7$ can be considered as a maximum extinction coefficient of water, at which return signals coming from underwater still differ from signals reflected from the land, provided that signals are averaged over several seconds while flying. For a single pulse this limit is even smaller.

3. MEASUREMENTS OF THE WATER TURBIDITY

The flight route near the Selenga delta is shown in Fig. 1 along with the 10- and 50-meter isobaths. The values of the extinction coefficient ϵ measured along the left part of the flight route before crossing the shore line (point 5 in Fig. 1) are shown in Fig. 3a. The arrows with the nearby figures 1, 2, ... indicate here the corresponding points of the flight route like in Fig. 1. The number of a lidar pulse is shown along the abscissa. The depth sharply decreases when flying between the points 2 and 3 and increases after flying over the point 7. The pulse repetition rate was initially 5 Hz (the first 1400 pulses), then it was increased up to 10 Hz. Every point in Fig. 3 corresponds to a single lidar pulse, and the bold curve shows the running averaging over 60 pulses. The two-coordinate distribution of the extinction coefficient near the Selenga mouth was constructed from these data; it is shown as grades of the gray scale in Fig. 4.

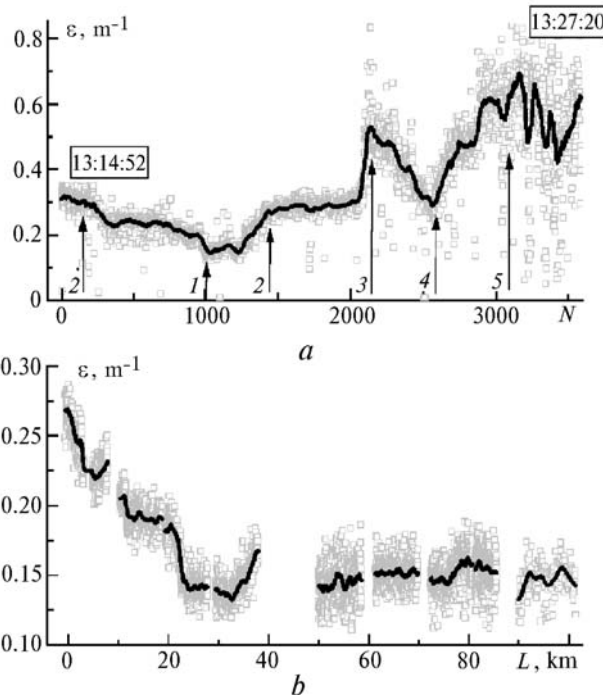


FIG. 3. Variation of the extinction coefficient along the route shown in Fig. 1.

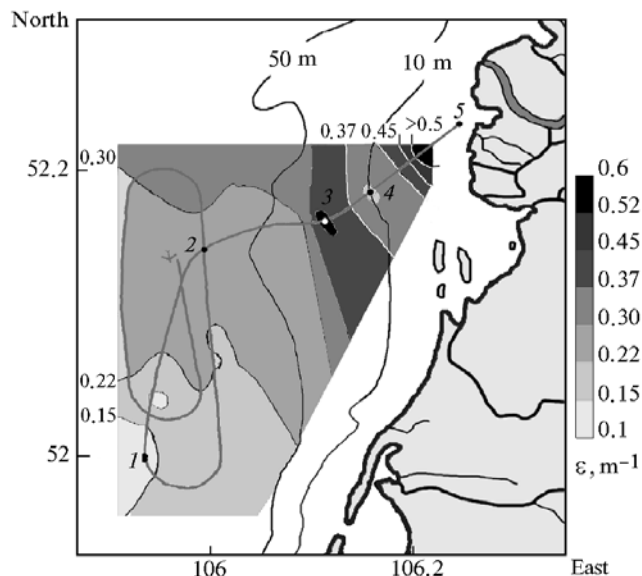


FIG. 4. Distribution of the extinction coefficient near the Selenga mouth. The values of the extinction coefficient are shown as grades of the gray scale. The isobaths of 10 and 50 m are shown for the lake bottom.

The minimum value of the extinction coefficient ϵ (0.14 m^{-1}) was observed in the section 1 of the route. As the mouth is approached (to the distance of 10 km from the mouth), the extinction coefficient increases monotonically up to the value of 0.35 m^{-1} . River Selenga carries a large amount of suspended clay particles, which sediment near the shore. The distinct boundary between

the river water and the pure lake water is seen even visually at the point 3 as a marked difference in the water color. When flying over this point, we have observed a sharp increase in the extinction coefficient up to $0.5\text{--}0.6\text{ m}^{-1}$. It is interesting that the extinction coefficient reduces back at the point 4. It is assumed that a flow of turbid water carried by one of the left branches of the river into the lake is observed to the left from the point 4. Starting from the point 5, laser pulses start to fall on the marshland of the Selenga delta.

While the aircraft flew away from the Selenga mouth (Fig. 3b corresponds to the flight route section from the point 7 shown in Fig. 1 to the north), water turbidity smoothly decreases. The pulse repetition rate for this section of the flight route was 5 Hz. The points in the figure are for single measurements, while the solid line demonstrates the averaging over 60 pulses, what corresponds to the distance of 1 km. More than 50 km far from Selenga (over the central part of Baikal) the values of ϵ drop down to $0.14\text{--}0.16\text{ m}^{-1}$. Much more transparent water ($\epsilon = 0.12\text{--}0.13\text{ m}^{-1}$) was observed in the northern part of Lake Baikal. Near the mouths of small rivers the water turbidity increases up to 0.25 m^{-1} .

4. SPATIAL SPECTRAL DENSITY OF FLUCTUATIONS IN THE EXTINCTION COEFFICIENT DUE TO WATER NEAR THE SELENGA MOUTH

The airborne measurements of laser radiation extinction in water using the method of lidar sensing allows the study of spatial structure of water transparency in the surface layer of Lake Baikal. The values of the extinction coefficient averaged over the flight route demonstrate a noticeable variability (which exceeds by several times the rms deviation from the mean value) in transparency of the water medium on the scales from several kilometers to several tens of kilometers. Within these scales, the continuous, in time, samples of the extinction coefficient were obtained. Fluctuations of the extinction coefficient allows estimation of the spatial characteristics of water mass dynamics.

These estimates are based on the assumption that the hydrosol, which is responsible for water transparency, is a conservative admixture carried under the effect of different-scale movements of water masses. Because the aircraft speed ($V_a = 80\text{ m/s}$) is far greater than the mean speed of water mass movements (tens cm/s), water masses can be considered "frozen" at the time of their airborne sensing. Therefore, we can use correctly enough the spatial presentation of the measured results instead of the temporal one.

To estimate the statistical parameters of the spatial structure, it is appropriate to consider only fluctuations of the extinction coefficient regardless of the absolute values. Therefore, let us transform the initial samples of values of the extinction coefficient into the new series having zero sampled mean and unit variance.

The initial data may contain trends or low-frequency components, the assumed period of which is far longer than the flight route length. With some discontinuous trends, joining of separate measurements into a continuous series will result in misestimates of the spectral characteristics. Therefore, such trends should be eliminated from the series having limited lengths. This elimination was performed by fitting of a low-order polynomial using the method of least squares.

Thus prepared series of experimental data is now a random process of fluctuation of the extinction coefficient about its zero mean with the unit variance. Low-frequency components, not fitting in the actually measured spatial scale of the length of a separate series, are eliminated from this process. The running median filter is applied to this series to smooth out high-frequency components caused by peaks due to instrumental and other errors in estimation of the extinction coefficient under conditions of low signal-to-noise ratio in the return signals.

The spatial structure of water mass movement in Lake Baikal can be studied using the standard methods of the spectral analysis from the set of initial data transformed in such a way.⁸ Let us describe the fluctuation process of the extinction coefficient in terms of spatial wavelengths λ . Then the spectral density $Sp_\epsilon(k)$ will be correspondingly determined from spatial wave numbers $k = 2\pi/\lambda$. The wavelengths were calculated based on the aircraft coordinates known from the GPS data accurate to 80 m and the aircraft velocity continuously controlled and stored in the computer along with the parallel fixation of the flight time.

The spectral density was calculated on the basis of the finite Fourier transform of the initial stationary random set of ϵ values determined in the finite region [$\lambda_0 < \lambda < L$], where $\lambda_0 = 2\Delta l$ is the minimum spatial scale determined by the resolution in a given case ($\Delta l = 15\text{ m}$); $L = N\Delta l$ is the maximum scale limited by the finite number n of the sample size in a given case. The Hahn temporal window was used to suppress percolation through the lateral maxima. To obtain the stable spectral estimate and to smooth out its value, the calculations by 50% overlapping segments were used. The initial joint sample with the size N is divided into n_d overlapping segments with the boundaries

$$q(i-1)L/(n_d-1) \leq \lambda \leq [q(i-1)+1]L/(n_d-1), \\ i = 1, 2, \dots, (n_d - q - 1), \quad q = 0.5.$$

The error in estimation of the spectral density $Sp_\epsilon(k)$ calculated in such a way is $\Delta\epsilon = 1/\sqrt{n_d}$. When a sample of ϵ values is divided into $n_d \cong N/100$ segments, $\Delta\epsilon$ averages to 10–20%. The spectral density of fluctuations in the extinction coefficient calculated using this method is shown in Fig. 5 in the double logarithmic scale. These results were obtained from the measurement data acquired near the Selenga mouth (Fig. 5a) and at some distance from the mouth in the north direction toward the lake center (Fig. 5b).

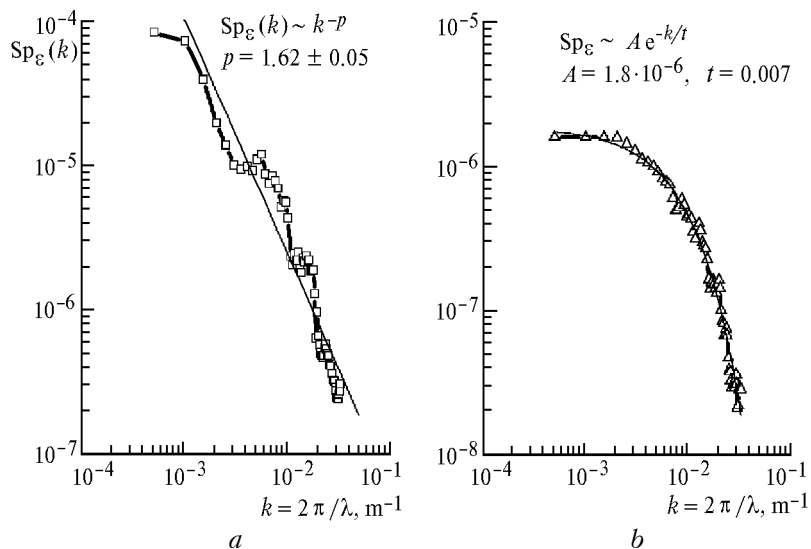


FIG. 5. Spatial spectra of fluctuations in the radiation extinction coefficient near the Selenga mouth (a) and to the north from the mouth (b).

The spectra are given for $30 < \lambda < 5000$ m spatial wavelength region. In this region, one can clearly see the marked difference in the distributions of the spectral densities of ϵ fluctuations due to possible streams, river water sink, vertical upward and downward flows, and turbulent mixing.

As seen from Fig. 5, the average energy of water mixing processes near the mouth, estimated from the variance of transparency fluctuations, is about two orders of magnitude higher than the energy of movement processes several tens kilometers far from the mouth. The wave number distribution of the spectral density of fluctuation energy (for Fig. 5a) can be approximated by the power law with the exponent -1.62 ± 0.05 . This value agrees well with the « $-5/3$ » law of the Kolmogorov–Obukhov theory for the inertia wavelength region, in which the stationary linear cascade of energy transfer from large-scale eddies to those of smaller-scale ones occurs. At the same time, the scales can be separated out in this spectrum ($\lambda_1 \sim 150$ m, $\lambda_2 \sim 70$ m), the process energy at which far exceeds the confidence “corridor” of values in the typical exponential fall off. The energy inflow from outside at these scales may be caused by friction of water masses against the bottom, whose depth is of the same scale.

The wave number distribution of the spectral density of energy fluctuations in the scale range under study (for Fig. 5b) is approximated by the exponential law with the approximating parameter equal to the mean variance of a process, that is $t = 0.007$ (the approximating expression is given in Fig. 5b). This shape of a spectrum is not typical of turbulent processes in oceanic waters. However, we have already detected it earlier when analyzing the data on water transparency in Lake Baikal.⁹ In that case, sensing was performed at a distance up to 10 km from the shore along the northern part of the lake. According to the theory of turbulence, this shape of the spectrum (see

Fig. 5b) is characteristic of the degenerating processes. The mean turbulence energy obtained in the river mouth area is carried by water movements of the scales of several hundred meters. At the same time, it becomes degenerating because of dissipation processes of interaction with the ambient water medium. The dissipation energy drops far faster than the inertial cascade process does for the same wave numbers.

5. BATHYMETRY

The minimal depth detectable with a lidar system depends at least on two factors: (a) the laser pulse duration Δl and the temporal resolution of the receiving system (we have $\Delta l = 3$ m), since if the depth $r < \Delta l$, then the pulse reflected from the water surface and the pulse reflected from the bottom cannot be resolved by the receiving system; and (b) the ratio between the return signal power and the dynamic range of the receiving system. In our measurements, when observing using a polarized radiation, all signals reflected from the bottom at a depth $r < 10$ m and return signals from the upper water layer cannot be resolved. However, the cross-polarized component of the return signal from upper water layers (in which the single scattering prevails) is small, while the return signal reflected from the bottom is depolarized almost completely. This increases sharply the contrast of the signal reflected from the bottom against the background of the signal scattered by the hydrosol. This situation is illustrated in Fig. 6, which demonstrates the lidar return (its cross-polarized component) received when flying over shallow water areas. The return signal intensity is shown using the grades of the gray scale (black color corresponds to the maximum return signal). The minimum detectable depth can be estimated as 4 m.

The maximum detectable depth (at the maximum sensitivity of the receiving system and the maximum laser power) depends, first of all, on water transparency. One

of the most interesting results obtained in the flight over B. Ushkanii Island is shown in Fig. 7. The maximum detectable depth here approaches 40 m (the right-hand part of the figure). The underwater extinction coefficient here is $\varepsilon = 0.127 \text{ m}^{-1}$, what corresponds to the visibility depth of the Secchi disc $Z_d = (3.5 - 7)/\varepsilon = (41 \pm 14) \text{ m}$ (these are the maximum

values of the transparency ever observed in Lake Baikal¹⁰). In the northern part of this group of islands, the measured depth approached 19 m at $\varepsilon = 0.184 \text{ m}^{-1}$, what corresponds to $Z_d = 28 \text{ m}$. When flying over the land, the profile of trees covering the island is clearly seen. However, this is a separate subject for a discussion.

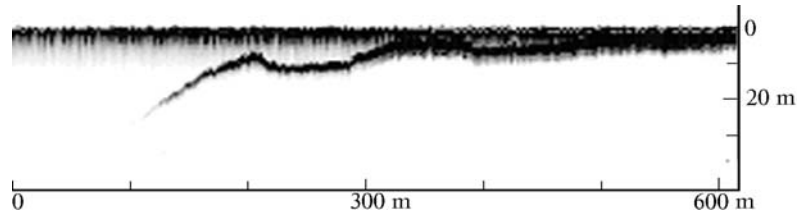


FIG. 6. Bathymetry in the area of smooth change of the lake depth.

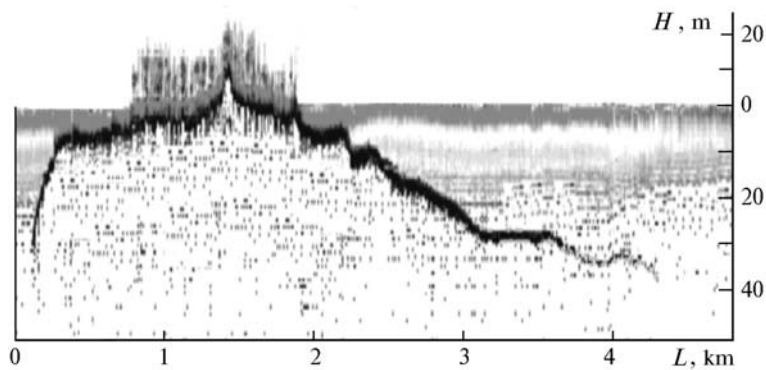


FIG. 7. The profile of the bottom, land height, and stand of trees recorded in one of the flights over Oshoi Ushkanii Island.

In accordance with the available geographic map, the depth near the Selenga mouth (at sections 3 and 4 of the flight route, see Fig. 1) equals 20 m and smoothly decreases. However, we failed to detect signals reflected from the bottom in this area. (Unfortunately, a more detailed bathymetric map of the lake is unavailable, and the lake in this area is likely to be deeper.) Another reason for this may be the vertical stratification of water turbidity. (The measured values of ε relate to only the upper water layer.) A possible increase in water turbidity near the bottom because of a continuous sedimentation of suspended particles carried by the river could result in a strong extra attenuation of a signal.

6. CONCLUSION

The results obtained show that the hydrooptical laser sensing can be used for solution of not only practical, but purely scientific problems as well. The measured power spectrum of fluctuations of the extinction coefficient for the Lake Baikal waters could

be compared, in some parameters, with similar spectra for sea waters. The peculiarities of such spectra could be used to distinguish among different types of water.

Our measurements have demonstrated that lidars are suitable for routine bathymetric measurements in shallow waters of lakes and seas. The methods to improve the accuracy of lidar signal processing with regard for peculiarities of pulse response of a receiving system have been worked out.

ACKNOWLEDGMENTS

The authors would like to express their gratitude to the crew of the AN-30 aircraft of Novosibirsk Airlines for excellent pilotage under severe environmental conditions of Lake Baikal. We are indebted to M.M. Krekova for fruitful discussions of our results.

The work was conducted in accordance with the Contract DERA ELM/1011 and partially supported by the Russian Foundation for Basic Research (Grant No. 97-05-96467).

REFERENCES

1. M.V. Panchenko, B.D. Belan, and V.S. Shamanaev, *Atmos. Oceanic Opt.* **10**, Nos. 4–5, 289–294 (1997).
2. G.P. Kokhanenko, I.E. Penner, and V.S. Shamanaev, *Atmos. Oceanic Opt.* **9**, No. 6, 484–488 (1996).
3. V.E. Zuev, B.D. Belan, D.M. Kabanov, et al., *Atmos. Oceanic Opt.* **5**, No. 10, 658–663 (1992).
4. A.I. Abramochkin, V.V. Zanin, I.E. Penner, A.A. Tikhomirov, and V.S. Shamanaev, *Opt. Atm.* **1**, No. 2, 92–96 (1988).
5. G.I. Vasilenko, *Theory of Signal Restoration* (Sov. Radio, Moscow, 1979), 272 pp.
6. A.N. Tikhonov, A.V. Goncharkii, V.V. Stepanov, and A.G. Yagova, *Regularizing Algorithms and A Priori Information* (Nauka, Moscow, 1983), 198 pp.
7. G.E. Forsythe, M.A. Malcolm, and C.B. Moler, *Computer Methods for Mathematical Calculations* (Prentice–Hall, Englewood Cliffs, New York, 1977).
8. J.S. Bendat and A.G. Piersol, *Random Data: Analysis and Measurement Procedures* (Wiley, New York, 1971).
9. I.E. Penner and V.S. Shamanaev, in: *Abstracts of Reports at the 17th Int. Laser Radar Conf.*, Sendai (1994), pp. 73–75.
10. P.P. Sherstyankin, in: *Optical Methods for Study of Oceans and Inland Water Areas*, G.I. Galaziya, ed. (Nauka, Moscow, 1979), pp. 16–27.